

Mathematical Modeling in Industry XII

## Stability of Extending Films

**Mentor:** Olus N. Boratav  
Corning Incorporated  
boratavon@corning.com

Jerome Goddard II  
Mississippi State University  
jg440@msstate.edu

Taebeom Kim  
University of Houston  
jklentzm@smu.edu

Jill Klentzman  
Southern Methodist University  
jklentzm@smu.edu

Dias Kurmashev  
University of Memphis  
dkurmshv@memphis.edu

Mauricio Osorio  
University of Cincinnati  
osorioma@email.uc.edu

Gregory Richards  
Kent State University  
grichard@math.kent.edu

August 15, 2008

## Abstract

The goal of this research is to revisit the stability results of Yeow (1974) on extending flows with free surfaces. The eigenvalue problem is formulated and solved for the flow of a Newtonian film such as the one encountered in film casting. The stable and unstable region boundaries is obtained. The analysis is extended to a non-isothermal case similar to the work by Shah and Pearson (1972) and German et al. (2006). Stability boundaries for different attenuation velocities (at the inlet and the exit of the process), and viscosity ratios are obtained. For the solutions which are unstable (or marginally unstable), time-dependent solutions (oscillating or growing in time) describing the free surface motion are obtained. The analysis which is applicable to a filament geometry is extended to a sheet with two length scales.

## Contents

<b>1</b>	<b>Introduction and Motivation</b>	<b>2</b>
<b>2</b>	<b>Filament Problem</b>	<b>3</b>
2.1	Formulation of Mathematical Model . . . . .	3
2.2	Steady State Solution . . . . .	5
2.3	Eigenvalue Problem . . . . .	10
2.4	Time-Dependent Solution . . . . .	13
<b>3</b>	<b>Sheet Problem</b>	<b>19</b>
3.1	Formulation of Mathematical Model . . . . .	19
3.2	Eigenvalue Problem . . . . .	21
<b>4</b>	<b>Recommended Future Work</b>	<b>24</b>
<b>5</b>	<b>Acknowledgements</b>	<b>24</b>

# 1 Introduction and Motivation

The main objective of this study is to understand the effects of increasing the thickness ratio of a flowing filament or sheet. In film casting or fiber spinning, the thickness ratio relates the thickness of the film at the inlet of the casting device to that at the outlet. An increased value of the thickness ratio can be a consequence of higher flow rates or a decrease in the final product thickness, both of which are often required to reach production goals. In this work, we analyze solutions by revisiting a filament geometry widely known in the literature, Yeow (1996), German et al. (2006), Suman et al. (2008), Pearson et al. (1969).

The main results in Howell (1996) are the identification of the relevant length and timescales for the buckling of viscous sheets and the derivation of new models for fully three-dimensional sheets of arbitrary geometry. The transition from stable to unstable solutions is examined as a function of a fixed Stokes number and a decreasing Stokes number. The eigen equation of this transition is used to reveal eigenvalues that change sign as the stability boundary is crossed. In addition, solutions of the time-dependent formulation of the problem show exponential growth in time with variables thickness or speed.

The filament analysis is extended to a geometry with two length scales and the solution approach is summarized.

## 2 Filament Problem

To generate thin filaments, a molten polymer is pumped through a circular opening in a metal plate and drawn down by axial tension. The thread then cools, solidifies and is wound on a spool, which provided the axial tension needed for the process (Matovich et al., 1969). We wish to study the stability of this process, particularly as it relates to the thickness ratio, or the ratio of the thickness of the film at the opening in the metal plate to the final thickness when it reaches the spool.

### 2.1 Formulation of Mathematical Model

To develop a mathematical model of the filament spinning process, we begin with the standard Navier-Stokes equations and continuity for an incompressible Newtonian liquid given by

$$\rho \left( \frac{\partial \vec{u}}{\partial t} + \vec{u} \cdot \nabla \vec{u} \right) = -\nabla p + \nabla \cdot \mu (\nabla \vec{u} + (\nabla u)^T) + \rho \vec{g}, \quad (2.1)$$

$$\nabla \cdot \vec{u} = 0, \quad (2.2)$$

with the coordinate system defined such that  $z$  is in the direction of the attenuation,  $r$  is in the radial direction of the cylindrical filament, and  $\theta$  is the azimuth, as shown in Figure 1. The velocity vector  $\vec{u}$  is given by  $\vec{u} = (u_r, u_\theta, u_z)$ ,  $\rho$  is the density of the liquid,  $p$  is the pressure, and  $\vec{g}$  is the acceleration due to gravity.

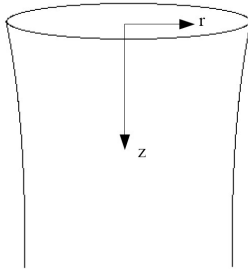


Figure 1: Filament diagram showing axis orientation.

We employ the stress balance at the filament-vapor interface,

$$\vec{T} \cdot \hat{n} = -\kappa \sigma \hat{n} + S \hat{t}, \quad (2.3)$$

where  $\vec{T}$  is the stress tensor,  $\kappa$  is the curvature,  $\sigma$  is the surface tension,  $S$  is the shear stress, and  $\hat{n}$  and  $\hat{t}$  are the outward unit normal and the tangent vectors to the interface, respectively. An additional boundary condition at the filament-air interface is the kinematic condition

$$u_r = \frac{\partial h}{\partial t} + u_z \frac{\partial h}{\partial z}, \quad (2.4)$$

where  $r = h(z)$  is the location of the filament-air interface. Because the radius of the filament is much smaller than the length of the filament in the  $z$ -direction, we take a lubrication-type approach to the problem, following the derivation given by Suman and Kumar (2008). We assume that the flow is axisymmetric and that  $u_\theta = 0$ . We scale the length in the  $r$ -direction by the radius of the filament at the inlet of the spinning device  $r_o$  and the length in the  $z$ -direction by the distance from the inlet of the spinning device to the outlet  $L$ . Pressure, viscosity, and the nonzero components of the velocity vector are scaled as

$$p = \frac{p}{\rho V_o^2}, \quad \mu = \frac{\mu}{\mu_o}, \quad u_z^* = \frac{u_z}{V_o}, \quad u_r^* = \frac{u_r L}{r_o V_o},$$

where the superscript “\*” denotes nondimensional quantities, and  $\mu_o$  and  $V_o$  are viscosity and the velocity in the  $z$ -direction at  $z = 0$ , respectively. All of the following formulations are in terms of the dimensionless quantities, though the “\*” is omitted for convenience. The velocity components and pressure are expanded as

$$\begin{aligned} u_z &= u_o(z, t) + (\epsilon r)^2 u_2(z, t) + O(\epsilon^4), \\ u_r &= -\frac{\partial u_o}{\partial z}(z, t) \frac{r}{2} - \frac{\partial u_2}{\partial z}(z, t) \frac{\epsilon^2 r^3}{4} - O(\epsilon^4), \\ p &= p_o(z, t) + p_2(z, t) (\epsilon r)^2 + O(\epsilon^4). \end{aligned} \quad (2.5)$$

We impose a temperature profile in the  $z$ -direction to simulate the presence of heaters surrounding the filament. The viscosity  $\mu$  is then expressed as a function of  $z$  rather than directly a function of temperature. The leading order governing equations and boundary conditions then give the following differential equations for the cross-sectional area of the filament  $A$ , neglecting the effects of shear stress:

$$ARe \left( \frac{\partial u_o}{\partial t} + u_o \frac{\partial u_o}{\partial z} \right) = \frac{\partial}{\partial z} \left( \mu(z) A \frac{\partial u_o}{\partial z} + C \sqrt{A} \right) + \frac{Re}{Fr} A, \quad (2.6)$$

$$\frac{\partial A}{\partial t} + \frac{\partial Au_o}{\partial z} = 0. \quad (2.7)$$

The important parameters that arise are the Reynolds number  $Re$ , Froude number  $Fr$ , inverse Capillary number  $C$ , and Stokes number  $Re/Fr$ , all of which are described in Table 1.

Symbol	Formula	Description	Typical Values
$Re$	$\frac{\rho LV_0}{3\mu_0}$	$\frac{\text{Inertia}}{\text{Viscous forces}}$	$10^{-5} - 10^{-3}$
$Fr$	$\frac{V_0^2}{gL}$	$\frac{\text{Inertia}}{\text{Gravity}}$	$10^{-5}$
$C$	$\frac{\sigma L}{3\mu_0 V_0 r_0}$	$\frac{\text{Surface Tension}}{\text{Viscous forces}}$	$10^{-4} - 10^{-2}$
$\frac{Re}{Fr}$	$\frac{\rho L^2 g}{3\mu_0 V_0}$	$\frac{\text{Gravity}}{\text{Viscous forces}}$	$1 - 32$

Table 1: Parameter formulas, definitions, and typical values used in this study.

## 2.2 Steady State Solution

We now have the filament problem in a nondimensional form. The first step to understanding our system and its behavior will be to study the solutions when all time derivatives are set to zero. That is, we will begin our investigation by looking at steady state solutions to the system:

$$(Au)_z = 0$$

,

$$\text{Re}(uu_z) = (\mu(z)Au_z + C\sqrt{A})_z + \frac{\text{Re}}{\text{Fr}}A$$

, for  $0 < z < 1$ , with boundary conditions

$$u(0) = A(0) = 1, \quad T_R = u(1)$$

, where  $T_R$  is the thickness ratio. The first of these two governing equations can be integrated to give

$$Au = c_1$$

for some constant  $c_1$ . By the boundary conditions, we can then infer that  $c_1 = 1$ . Thus,

$$A = \frac{1}{u}.$$

. Substituting this new relation between  $A$  and  $u$  back into our differential equation and making the simplifying assumption that  $\text{Re} \cong C \cong 0$ , we now have the final formulation of the steady-state problem:

$$\left( \mu(z) \frac{u_z}{u} \right)_z = \frac{\text{Re}}{\text{Fr}} \cdot \frac{1}{u}, \quad 0 < z < 1,$$

$$u(0) = 1, \quad T_R = u(1).$$

This is a non-linear two-point boundary value problem that MATLAB's `bvp4c()` was designed to handle. MATLAB's `bvp4()` is designed to solve ODE's in the form

$$\mathbf{y}' = \mathbf{f}(x, \mathbf{y}), \quad a < x < b,$$

$$\mathbf{g}(\mathbf{y}(a), \mathbf{y}(b)) = 0.$$

Now, our problem is in the form

$$u_{zz} = f(u, u_z), \quad 0 < z < 1.$$

So, to get the required form, we define

$$\mathbf{y}(z) = \begin{pmatrix} u \\ u_z \end{pmatrix}, \quad \mathbf{f}(z, \mathbf{y}) = \begin{pmatrix} y_2 \\ h(y_1, y_2) \end{pmatrix}, \quad \mathbf{g}(\mathbf{y}(0), \mathbf{y}(1)) = \begin{pmatrix} 1 - y_1(0) \\ T_R - y_1(1) \end{pmatrix},$$

where  $h(y_1, y_2)$  is defined by

$$h(y_1, y_2) = \frac{1}{\mu(z)} \left( \mu_z(z) y_2 + \mu(z) \frac{y_2^2}{y_1} + \frac{\text{Re}}{\text{Fr}} \right).$$

Recalling that we are imposing a temperature curve, and thereby imposing a viscosity curve,  $\mu(z)$ , we have a well-posed problem with several physical parameters that should vary the behavior of the system. In the next section we shall look at how the velocity and the thickness profile behave as a result of varying  $T_R$ ,  $\frac{\text{Re}}{\text{Fr}}$ , and  $\mu(z)$ .

Before we continue on to the results of our numerical investigation, we will take some time to discuss our choice of  $\mu(z)$  curves. Our requirements for choosing a viscosity curve were that  $\mu(0) = 1$  and  $\mu(1) = B$ , where  $B$  is some constant to be determined. We also felt that it would be useful to have some control over the rate and shape of the curve. To this end, we chose

$$\mu(z) = e^{rx} + \frac{e^{rx} - 1}{e^r - 1} \cdot (B - e^r).$$

This viscosity curve allows us to observe different phenomenon that the system undergoes for different heating and cooling curves.

To investigate steady state behavior, we first consider a constant viscosity,  $\mu = 1$ , followed by two monotonically increasing viscosity functions,  $\mu = \mu_1(z)$  and  $\mu = \mu_2(z)$ . Figure 2 shows  $\mu_1(z)$  and  $\mu_2(z)$  plotted vs  $z$ . Notice that  $\mu_1(z)$  reaches a high viscosity level quickly and then begins to level out, whereas  $\mu_2(z)$  remains small and then spikes as  $z$  approaches 1. For the constant viscosity case, Figure 3 presents the radius profile for various thickness ratios. We observe that for small thickness ratios, the radii decrease almost linearly, but for larger values, they become nonlinear, concave-up curves.

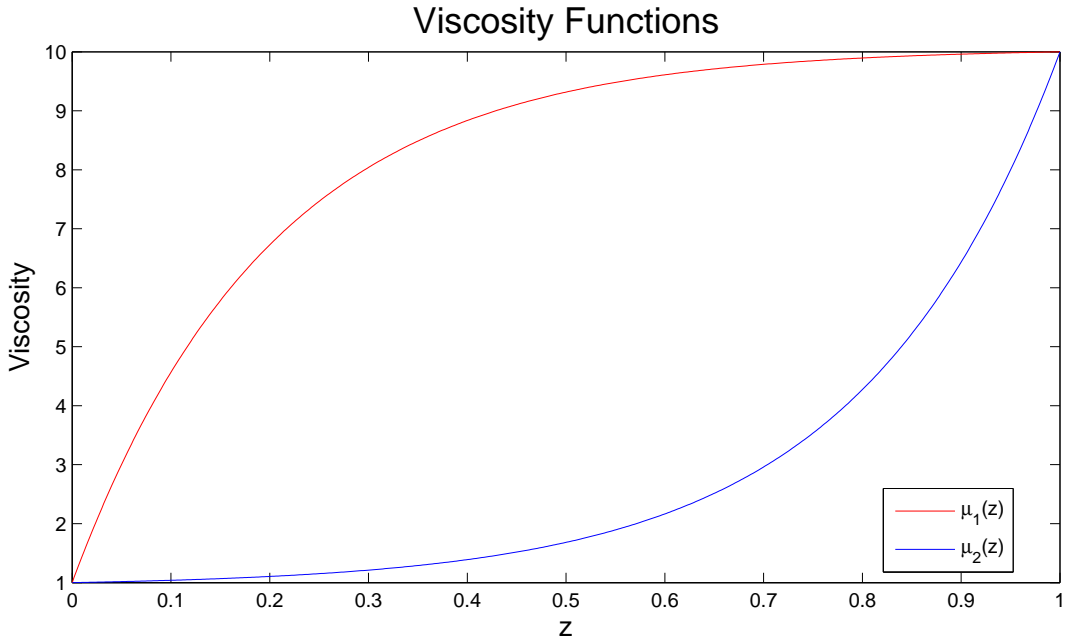


Figure 2: Several viscosity functions applied in this study.

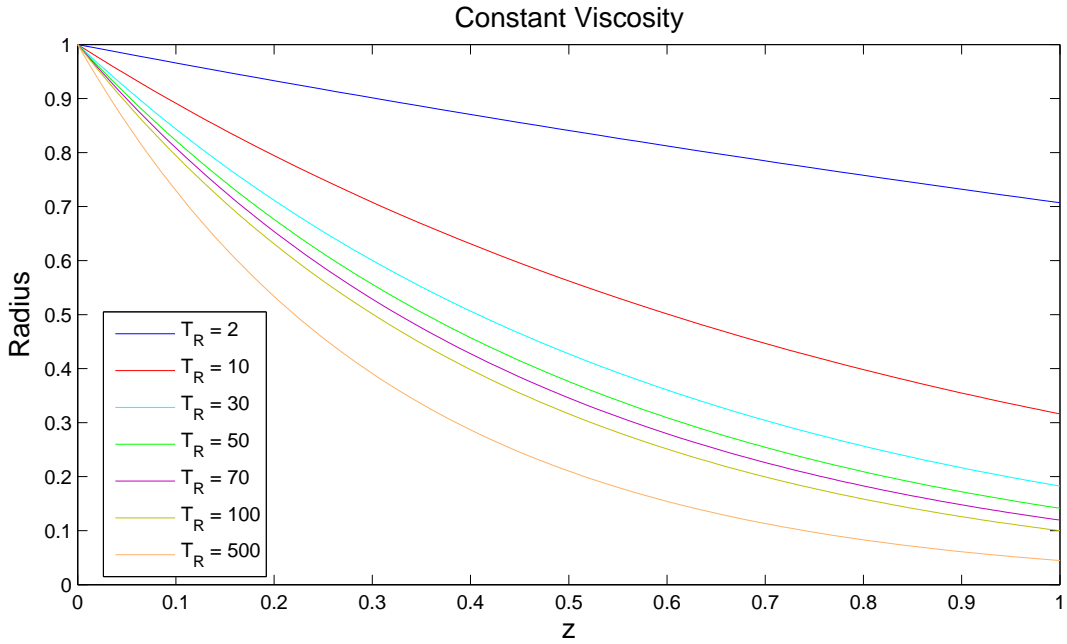


Figure 3: Radius vs  $z$  for various thickness ratios with  $\mu = 1$ .

In figure 4, the radius profile is presented again for different thickness ratios. In this case, the curves all have a similar nonlinear, concave-up shape. The radii decay quickly for small  $z$ -values, followed by a slower decrease as  $z$  approaches 1. This is due to the structure of  $\mu_1(z)$ , i.e. higher viscosity in a region causes a larger-magnitude decay. We observe that for all thickness ratios, the final radius is comparable to the constant viscosity case. Figure 5 shows the radius profile using  $\mu_2(z)$ . In this case, the initial shape of the curves are very similar to those in Figure 2. However, as  $z$  approaches 1, the higher viscosity of  $\mu_2(z)$  function again causes a drop in the final radius of each curve. Interestingly, changing the viscosity does not seem to have a radical effect on the overall shape of the curves.

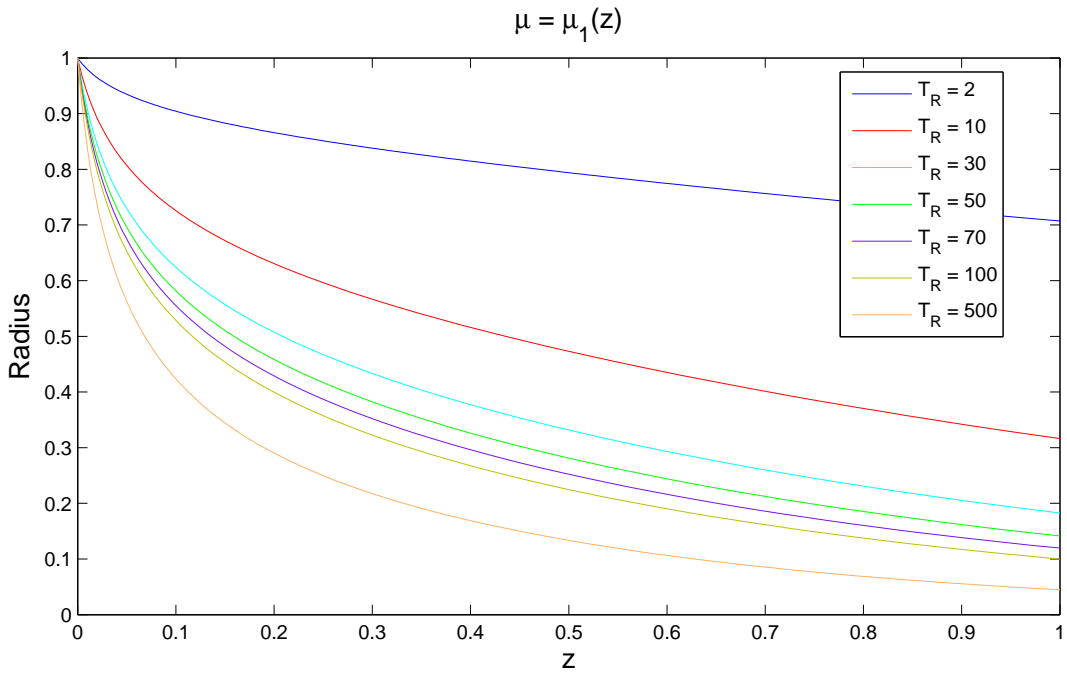


Figure 4: Radius vs  $z$  for various thickness ratios with  $\mu = \mu_1(z)$ .

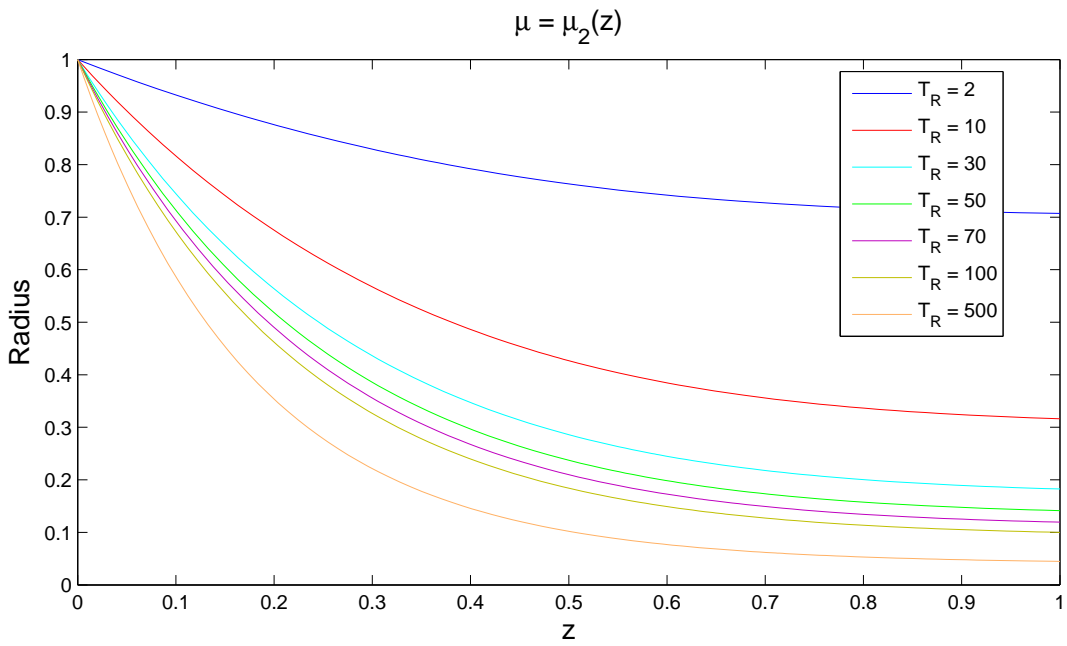


Figure 5: Radius vs  $z$  for various thickness ratios with  $\mu = \mu_2(z)$ .

Finally, Figure 6 presents starting force, the force at  $z = 0$ , vs thickness ratio for  $\mu = 1$ ,  $\mu_1(z)$ , and  $\mu_2(z)$ . We note that overall, higher viscosity yields a larger initial force. In all three cases, a thickness ratio of 1 yields no initial force. This supports the conclusion that higher viscosity results in a reduction in the stability.

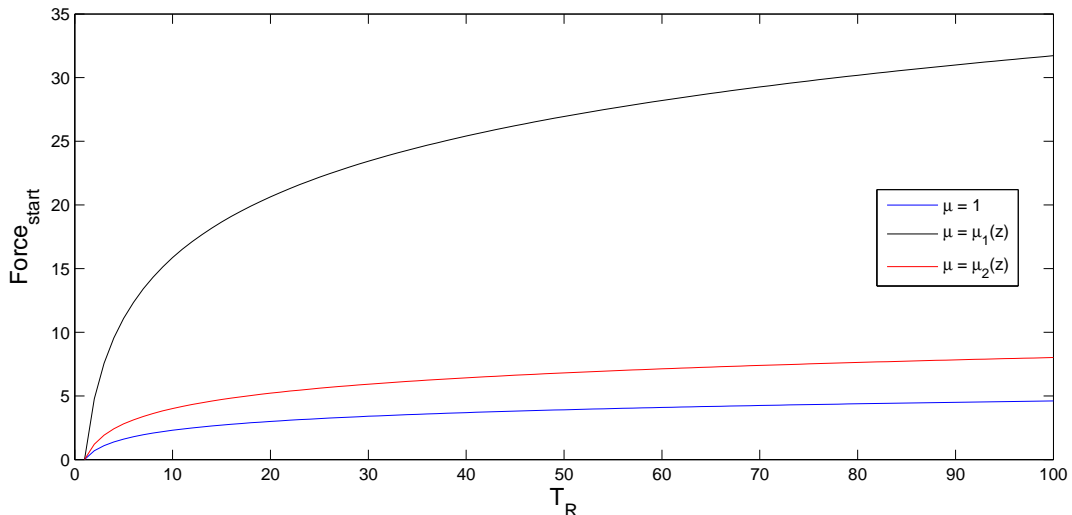


Figure 6: Starting Force vs  $z$  for  $\mu = 1$ ,  $\mu = \mu_1(z)$ , and  $\mu = \mu_2(z)$ .

Now that we have studied the steady state solution of the filament problem and have done some numerical exploration of the effects of the physical parameters on the thickness and velocity curves, we would like to know if those solutions are stable with regard to small or large perturbations. To this effect, we will look at two different ways to determine the stability of the solution. First we will explore a linearized eigenvalue problem followed by a scheme of perturbing the steady state solution and examining how the solution evolves in time by solving the full time-dependent problem.

### 2.3 Eigenvalue Problem

The first and probably the easiest approach to study the stability of the steady states is through a linear stability analysis. For this, we express each variable in the following way (notice that the possibility of perturbations in azimuthal and radial directions is not considered):

$$u(z, t) = \widehat{u}(z) + \widetilde{u}(z)e^{\lambda t}, \quad (2.8)$$

$$A(z, t) = \widehat{A}(z) + \widetilde{A}(z)e^{\lambda t}, \quad (2.9)$$

where we use hats to denote steady-state solutions and tildes to denote a small-amplitude perturbation term. Here also  $\lambda$  is the growth rate of the perturbation. Upon substitution of expressions (2.8) and (2.9) into our filament model (equations 2.6 and 2.7), and after linearization, the perturbation variables are found to satisfy the following differential equations:

$$\lambda \widetilde{A} + (\widehat{u}\widetilde{A} + \widetilde{u}\widehat{A})_z = 0, \quad (2.10)$$

$$\begin{aligned} Re(\lambda \widetilde{u}\widehat{A} + \widetilde{A}\widehat{u}_z\widetilde{u} + \widehat{u}\widetilde{u}_z\widehat{A} + \widetilde{A}\widetilde{u}\widehat{u}_z) &= [\mu(z)\widehat{A}\widetilde{u}_z + \mu(z)\widetilde{A}\widehat{u}_z]_z \\ &+ \frac{Re}{Fr}\widetilde{A} + \frac{C}{\sqrt{\widehat{A}}}(\widetilde{A}_z - \frac{\widehat{A}_z}{2\widehat{A}}\widetilde{A}). \end{aligned} \quad (2.11)$$

This system of linear homogeneous equations constitutes an eigenvalue problem, where  $\lambda$  is the complex eigenvalue in it (the real part being the growth or decay rate, and the imaginary part, the disturbance frequency). The boundary conditions are:  $\widetilde{u}(0) = 0$ ,  $\widetilde{A}(0) = 0$ , and  $\widetilde{u}(1) = 0$ .

A variety of methods can be applied to solve the eigenvalue problem, most of which treat it as an initial-value problem and solve it numerically using finite differences. Using that approach, with backward differences to approximate first order spatial derivatives, central differences to approximate second order spatial derivatives, and considering  $Re = C = 0$ , we find:

$$\begin{aligned} \lambda \widetilde{A}_i + \frac{(\widehat{u}_i\widetilde{A}_i + \widetilde{u}_i\widehat{A}_i) - (\widehat{u}_{i-1}\widetilde{A}_{i-1} + \widetilde{u}_{i-1}\widehat{A}_{i-1})}{h} &= 0, \\ \mu'_i\widehat{A}_i\frac{\widetilde{u}_i - \widetilde{u}_{i-1}}{h} + \mu_i\frac{\widetilde{u}_i - \widetilde{u}_{i-1}}{h}\frac{\widehat{A}_i - \widehat{A}_{i-1}}{h} + \mu_i\widehat{A}_i\frac{\widetilde{u}_{i+1} - 2\widetilde{u}_i + \widetilde{u}_{i-1}}{h^2} \\ + \mu'_i\widetilde{A}_i\frac{\widehat{u}_i - \widehat{u}_{i-1}}{h} + \mu_i\frac{\widehat{u}_i - \widehat{u}_{i-1}}{h}\frac{\widetilde{A}_i - \widetilde{A}_{i-1}}{h} + \mu_i\widetilde{A}_i\frac{\widehat{u}_{i+1} - 2\widehat{u}_i + \widehat{u}_{i-1}}{h^2} + \frac{Re}{Fr}\widetilde{A}_i &= 0, \end{aligned}$$

where  $h$  denotes the mesh size (uniform) of the spatial discretization, and  $i = 1, 2, \dots, n$ , for  $n = \frac{1}{h} - 1$ . From this we obtain:

$$\lambda A + M_1 A + M_2 U = 0, \quad (2.12)$$

$$B_1 A + B_2 U = 0, \quad (2.13)$$

where  $A = [A_1 \ A_2 \ \dots \ A_n]'$ ,  $U = [u_1 \ u_2 \ \dots \ u_n]'$ , and  $M_1, M_2, B_1, B_2$  are  $n \times n$  bi- or tridiagonal matrices containing information about the steady state solution.

Thus, after the substitution of equation (2.13) into (2.12) we get the eigenvalue problem:  $MA = \lambda A$ , with  $M = M_2 B_2^{-1} B_1 - M_1$ . This procedure was implemented in MATLAB to obtain the leading eigenvalue (largest real part) of the matrix  $M$ . The results are independent of the numerical method used (different finite differences schemes) but are slightly sensitive to the number of nodes. It is worth mentioning that the results obtained are close to those reported in Wyley *et al.* (1996) and Suman & Kumar (2008).

To analyze the stability behavior, the real part of the leading eigenvalue has been plotted as a function of the thickness ratio (Figure 7).

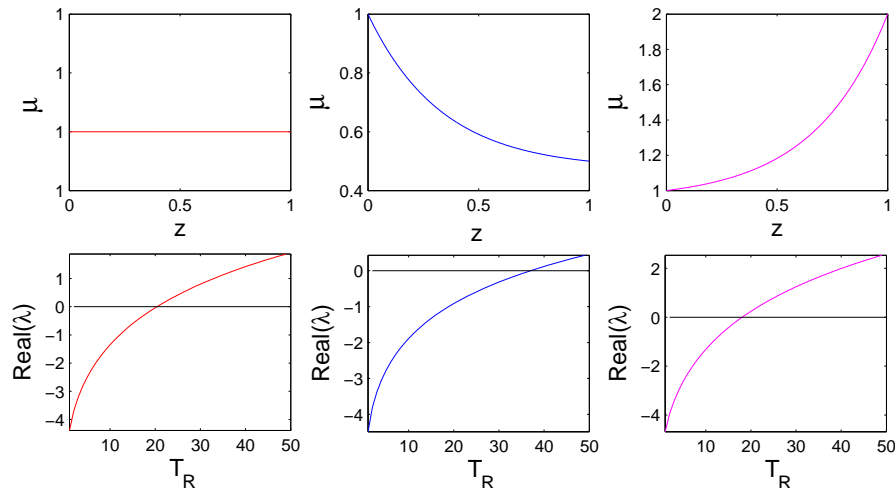


Figure 7: Critical thickness ratio vs Stokes number.

Now that we have an implementation of a linear stability scheme, we can utilize said scheme to numerically investigate the system. Even though the eigenvalues are sensitive to the number of nodes used in discretization, the trends of the eigenvalues with respect to other physical parameters is fairly robust. To that end we have used the linear stability model to investigate the change in the crossover thickness ratio with respect to varying the Stokes number,  $\text{Re}/\text{Fr}$ .

The results are displayed in Figure 8. Here we can see that the general trend is that an increase in Stokes number causes an increase in the critical

draw ratio. It is important to note, however, that the smallest critical ratio in the middle graphs (which represent the addition of a heating source) is about twice as large as the smallest critical ratio in the far left graphs, representing a constant viscosity curve. Thus we can see that by adding a heating source, a larger thickness ratio can be obtained.

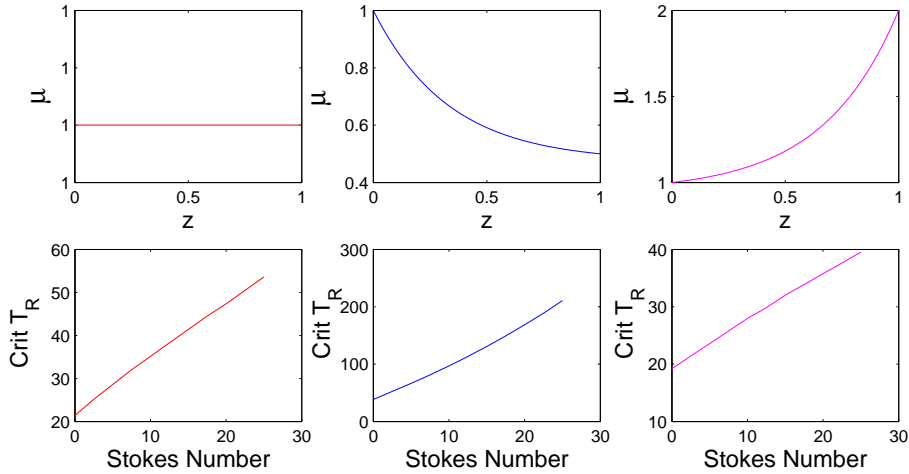


Figure 8: Critical thickness ratio vs Stokes number.

## 2.4 Time-Dependent Solution

Though we have an eigenvalue scheme to study the stability of our steady state solutions, we would like to know how both the stable and unstable solutions behave as a function of time. Studying the time-dependent solution numerically should also allow us to confirm the results of our eigenvalue scheme.

To this end, we now go back to the full system of equations

$$A_t + (Au)_z = 0,$$

$$(\mu(z) Au_z)_z + \frac{\text{Re}}{\text{Fr}} A = 0.$$

Because we are ignoring the inertial forces, a time derivative only appears in our first equation. This allows us to use a more ad-hoc approach when solving this system. The basic overview of our scheme is as follows, where

superscripts are used to denote the time variable, and subscripts are used to denote the space variable:

- Solve the steady state problem.
- Perturb the steady state solution slightly, or not so slightly, depending on the affect we desire.
- Take an Euler Step in the time direction by estimating

$$A_i^{n+1} \cong \frac{k}{h}(A_{i-1}^n u_{i-1}^n - A_i^n u_i^n),$$

where  $k$  is the time step and  $h$  is the spacial step. Here we used upwinding due to the velocity direction in our problem.

- Estimate  $u^{n+1}$  by solving

$$\mu'_i A_i \cdot \frac{u_{i+1}^{n+1} - u_{i-1}^{n+1}}{2h} + \mu_i \cdot \frac{A_{i+1}^{n+1} - A_{i-1}^{n+1}}{2h} \cdot \frac{u_{i+1}^{n+1} - u_{i-1}^{n+1}}{2h} + \mu_i A_i \frac{u_{i+1}^{n+1} - 2u_i^{n+1} + u_{i-1}^{n+1}}{h^2} + \frac{\text{Re}}{\text{Fr}} A_i = 0.$$

- Repeat Steps 3 and 4 ad infimum or until some stopping criteria has been reached.

Though this method led us to some interesting numerical data, and our data converged as we decreased the time step and increased the grid points in our spacial dimension, our scheme is not without short comings. Since we have used an explicit method, the spacial grid size can only be increased to a certain point before the time step must be decreased. Thus if we required very accurate results, our current method would take a significant amount of computing time. Instead of an Euler step, we could implement an implicit method to enable us to take a larger time step. In addition, we could implement an adaptive time step to lessen the number of steps required to reach a steady state after the perturbation, since for a steady solution most of the dramatic change of the system occurs close to  $t = 0$ .

With or without these improvements, the time-dependent solution method has several benefits over the eigenvalue scheme. The eigenvalue scheme is based on a linearization of a small amplitude perturbation. Because we introduce our perturbations numerically in the time-dependent case, we can study the effects of both small and large perturbations. In addition we can study the effects of several types of perturbations. For example, we could

introduce an increase in the exit velocity of the material or a sinusoidal variation to the thickness curve. In this report, we will concentrate on an increase to the exit velocity of the material.

As a first approximation, we have decided on a simple step function to increase the exit velocity by 30% as shown in Figure 9.

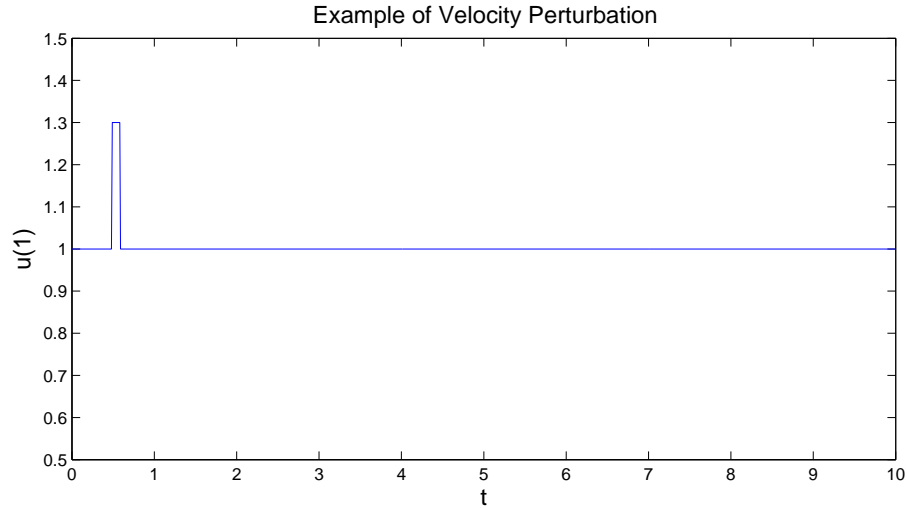


Figure 9: Velocity perturbation.

We investigated several phenomenon with the time-dependent solution. The first and most interesting phenomenon was the fact that we can find a thickness ratio that is unstable with a constant viscosity that becomes stable when a heating curve is applied. This occurrence can be seen in figures 10, 11, and 12. The first figure shows the time evolution of the steady state solution with constant viscosity and a thickness ratio of 50. Here we can plainly see the instability evolve. Figure 11 shows the same system but with a heating curve, where the viscosity is increased by a factor of 2. As one can see, this heating curve changes the instability of the constant viscosity case to a stable curve. The final figure shows the effects of a cooling curve. We notice that this curve also has an unsteady solution.

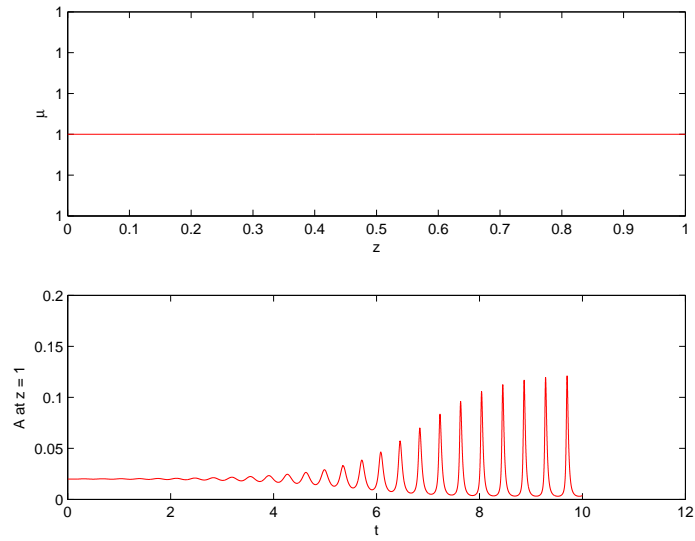


Figure 10:  $A$  vs  $t$  for constant viscosity.

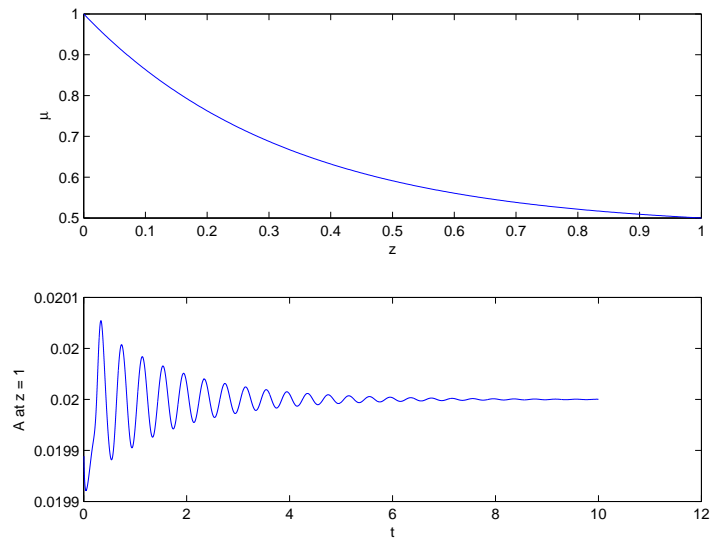


Figure 11:  $A$  vs  $t$  with a heating source.

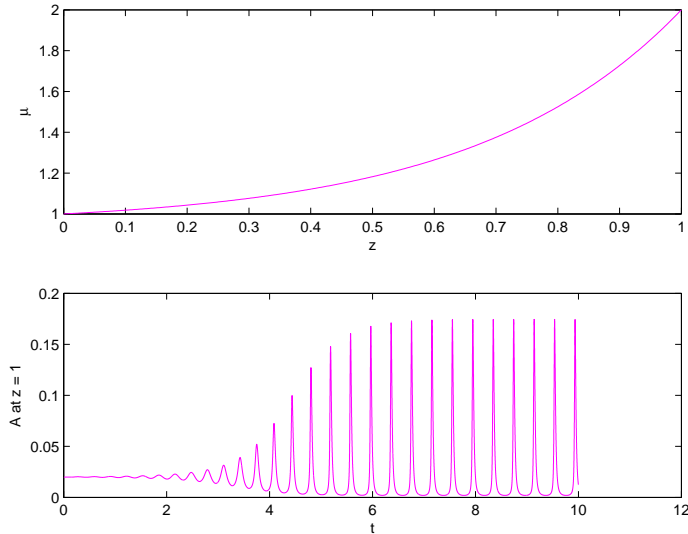


Figure 12: A vs t with a cooling source.

At this point it behooves us to mention that the eigenvalue scheme and the time dependent method do not agree numerically for the crossover thickness ratio from stable to unstable. We have seen that by increasing the number of grid points in the spacial direction, the time-dependent method tends towards the value given by the eigenvalue scheme and with previous results. We believe that if we had time to compute a very fine spatial grid along with a very small ( $\approx 10^{-6}$ ) time step, the results would agree.

Since our model has been nondimensionalized, the only control we have over the absolute viscosity is by changing the value of  $Re/Fr$ , the Stokes number term. This term contains the initial viscosity in its denominator. Thus by raising the Stokes number we can investigate the effects of having a lower absolute viscosity, and by raising the Stokes number we can investigate the opposite effect. This was the second phenomena we investigated with the time-dependent method. In Figure 13, we show similar figures to Figures 10, 11, and 12 for a higher Stokes number. We notice that all three curves are stable with a thickness ratio of 50. These results agree with previous investigations that showed that by decreasing the absolute viscosity the system becomes more stable overall.

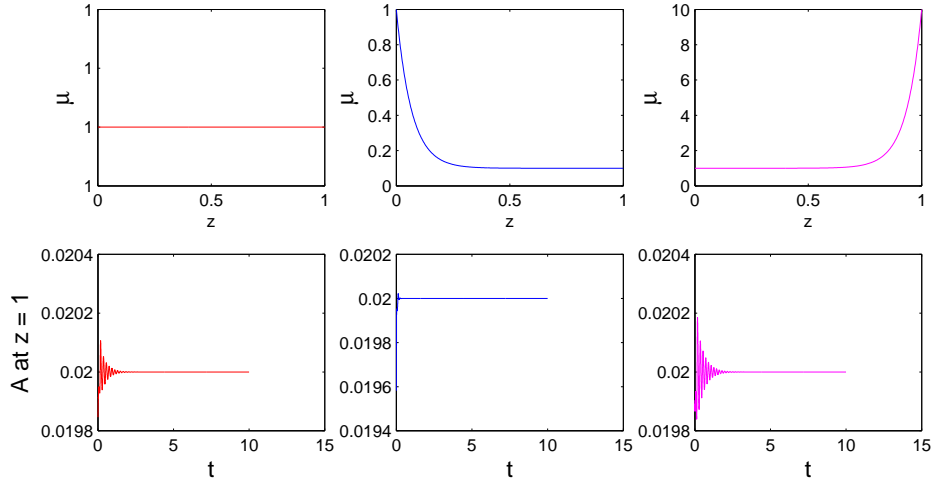


Figure 13:  $A$  vs  $t$  for a Stokes number of 50 with varying viscosities.

In conclusion, studying the filament problem has given us a wealth of insight into the stability of extending flows. Even with a simplified one-dimensional model, we were able to capture many of the physical properties of the system. We saw the effect of a viscosity curve to the shape of the film and the pulling force. We used our eigenvalue scheme to discover whether a steady state solution is stable or not. We also used this scheme with a binary search to find the critical thickness ratio. We were then able to study the effects of heating and cooling on the critical ratio as well as the effects that increasing the Stokes number has the critical ratio. Finally, we used a perturbation and time step method to further investigate the stability and the evolution of the thickness profiles, both stable and unstable.

### 3 Sheet Problem

Film casting is the process by which a molten polymer is stretched into thin sheets in air and then cooled on a chill roller, as described by Lamberti (2001). Mathematical analysis of this procedure is similar to that of fiber spinning but with the additional challenge of a significant length in the transverse direction, rather than the axisymmetry involved in the fiber problem. Appropriate simplifying assumptions must be made to produce a viable mathematical model that can be used to analyze the stability of the steady state solution with a given thickness ratio.

#### 3.1 Formulation of Mathematical Model

To develop a mathematical model of the sheet, we follow a similar formulation to that of the filament problem but with a Cartesian coordinate system, defined in Figure 14. We begin with the Navier-Stokes equations for momentum and mass conservation given by

$$\rho(\partial_t \mathbf{u} + \mathbf{u} \cdot \nabla \mathbf{u}) = -\nabla p + \nabla \cdot \mathcal{T} + \rho g \mathbf{e}_y, \quad (3.1)$$

$$\nabla \cdot \mathbf{u} = 0, \quad (3.2)$$

where  $\mathbf{u} = (u, v, w)$  is the velocity vector,  $\mathcal{T} = \mu(\nabla \mathbf{u} + (\nabla \mathbf{u})^T)$  is the total stress tensor,  $\partial_t$  is the time derivative,  $p$  is the pressure,  $\mathbf{e}_y$  is the unit vector in the  $y$ -direction,  $g$  is the gravitational constant and  $\rho$  is the density. The stress balance at the liquid-air interface is

$$(-p\mathbf{I} + \mu\mathcal{T}) \cdot \mathbf{n} = -\kappa\sigma\mathbf{n} + S\mathbf{t}, \quad (3.3)$$

where  $\mathbf{n}$  is the outward unit normal vector to the surface,  $\kappa$  is twice the mean curvature,  $\sigma$  is the surface tension,  $S$  is the external shear stress, and  $\mathbf{t}$  is the unit tangent vector.

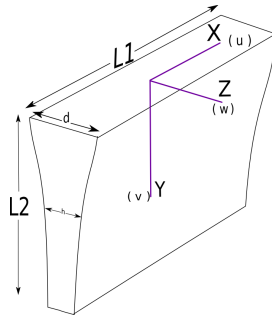


Figure 14: Sheet diagram showing axis orientation.

For the highly viscous fluids, such as the materials relevant to this study, the Reynolds number is very small,  $\text{Re} \ll 1$ , which makes the left-hand side of the Navier-Stokes equation negligible, giving

$$0 = -\nabla p + \nabla \cdot \mathcal{T} + \rho g \mathbf{e}_y. \quad (3.4)$$

Based on the physical construction of the problem, we make the following assumptions:

$$\begin{aligned} u &= u(x, y, t), & v &= v(x, y, t), \\ w &= w(x, z, t), & \mu &= \mu(y). \end{aligned}$$

This leads us to

$$\mu_y(u_y + v_x) + \mu(2u_{xx} + u_{yy} + v_{xy} + w_{xz}) = 0, \quad (3.5)$$

$$2\mu_y v_y + \mu(u_{yx} + v_{xx} + 2v_{yy} + w_{yz}) = \rho g, \quad (3.6)$$

$$\mu_y w_y + \mu(w_{xx} + w_{yy} + 1w_{zz}) = 0. \quad (3.7)$$

Because the thickness of the sheet in the  $z$ -direction is much smaller than all other length scales in the problem, we let  $\epsilon = d/L \ll 1$  and perform an asymptotic expansion in terms of  $\epsilon$ . We let  $\gamma = L_1/L_2$  be an order one quantity and scale the length and velocity components such that

$$\begin{aligned} x^* &= \frac{x}{\gamma L_2}, & y^* &= \frac{y}{L_2}, & z^* &= \frac{z}{\epsilon L_2}, \\ u^* &= \frac{\gamma u}{V}, & v^* &= \frac{v}{V}, & w^* &= \frac{w}{\epsilon V}, \end{aligned}$$

where  $V = v(0, 0, 0)$  and the superscript “\*” denotes dimensionless quantities. We scale the viscosity  $\mu$  by  $\mu_0$ , the viscosity at  $y = 0$ . With these scalings, the leading order nondimensional system is

$$\mu_{y^*}(u_{y^*}^* + v_{x^*}^*) + \mu\left(\frac{2}{\gamma^2}u_{x^*x^*}^* + u_{y^*y^*}^* + v_{x^*y^*}^* + w_{x^*z^*}^*\right) = 0, \quad (3.8)$$

$$2\mu_{y^*}v_{y^*}^* + \mu\left(\frac{1}{\gamma^2}u_{x^*y^*}^* + \frac{1}{\gamma^2}v_{x^*x^*}^* + 2v_{y^*y^*}^* + w_{y^*z^*}^*\right) = \frac{\rho g L^2}{V \mu_0}, \quad (3.9)$$

$$2\mu w_{z^*z^*}^* = 0. \quad (3.10)$$

With the additional assumption that viscosity is constant and that the effects of gravity are negligible, Howell (1996) applies the appropriate leading order boundary conditions to this system to obtain the following governing equations for the nondimensional thickness of the film  $h$ :

$$h_t + (uh)_x + (vh)_y = 0, \quad (3.11)$$

$$[2h(2u_x + v_y)]_x + [h(u_y + v_x)]_y = 0, \quad (3.12)$$

$$[2h(2u_x + v_y)]_y + [h(u_y + v_x)]_x = 0. \quad (3.13)$$

All of the variables in the above equations are nondimensional, with the superscript “\*” dropped for convenience. It is interesting to note that the one-dimensional version of Howell’s model, which considers a sheet of infinite length in the  $x$ -direction, is very closely related to the fiber model. The equations governing the thickness  $h$  of the infinite sheet in Howell’s model directly correspond with the equations governing the cross-sectional area  $A$  of the fiber when the same assumptions about a small Reynold’s number are applied, as mentioned in Howell (1996). Thus, the numerical simulations and eigenvalue analysis performed on the fiber problem can be related to the sheet problem for sections of the sheet far from the boundaries in the  $x$ -direction.

## 3.2 Eigenvalue Problem

Similar to the filament problem, if we could find a steady state solution to the two dimensional sheet problem we should then perform stability analysis on those solutions. To this end, we have formulated a linearized stability analysis problem that is then reduced to an eigenvalue problem. We start with the steady state system

$$(uh)_x + (vh)_y = 0,$$

$$[2h(2u_x + v_y)]_x + [h(u_y + v_x)]_y = 0,$$

$$[h(u_y + v_x)]_x + [2h(u_x + 2v_y)]_y = 0.$$

To make the notation of this system more manageable, we define the following differential operators

$$\begin{aligned} L_1(h, u, v) &= (uh)_x + (vh)_y, \\ L_2(h, u, v) &= [2h(2u_x + v_y)]_x + [h(u_y + v_x)]_y, \\ L_3(h, u, v) &= [h(u_y + v_x)]_x + [2h(u_x + 2v_y)]_y. \end{aligned}$$

With these definitions our steady state problem becomes

$$L_i(h, u, v) = 0, \quad i = 1, 2, 3.$$

It will benefit us to take a moment to discuss one property of these operators. We can show that all the differential operators defined above are linear in the first component and linear in the second and third component. That is,

$$L_i(\alpha h_1 + \beta h_2, u, v) = \alpha L_i(h_1, u, v) + \beta L_i(h_2, u, v),$$

and

$$L_i(h, \alpha u_1 + \beta u_2, \alpha v_1 + \beta v_2) = \alpha L_i(h, u_1, v_1) + \beta L_i(h, u_2, v_2).$$

Now, assume that  $(\hat{h}, \hat{v}, \hat{u})$  is a solution to steady state problem. Next we define  $h, v, u$  to be a solution to the steady state plus a small amplitude perturbation. Let

$$h = \hat{h} + \tilde{h}e^{\lambda t}, \quad v = \hat{v} + \tilde{v}e^{\lambda t}, \quad u = \hat{u} + \tilde{u}e^{\lambda t}. \quad (3.14)$$

Substituting (3.14) into equations (3.14), and using the fact that the perturbations are of small amplitude, we can see that

$$\begin{aligned} \lambda \tilde{h} + L_1(\tilde{h}, \hat{u}, \hat{v}) + L_1(\hat{h}, \tilde{u}, \tilde{v}) &= 0, \\ L_2(\tilde{h}, \hat{u}, \hat{v}) + L_2(\hat{h}, \tilde{u}, \tilde{v}) &= 0, \\ L_3(\tilde{h}, \hat{u}, \hat{v}) + L_3(\hat{h}, \tilde{u}, \tilde{v}) &= 0, \end{aligned}$$

If we let  $H, U, V$  be discretization vectors of  $\tilde{h}, \tilde{u}, \tilde{v}$ . Then the problem (3.15) can be represented as

$$\lambda H + A_1 U + A_2 V = 0, \quad (3.15)$$

$$B_1 H + B_2 U + B_3 V = 0, \quad (3.16)$$

$$C_1 H + C_2 U + B_3 V = 0, \quad (3.17)$$

where  $A_i, B_i, C_i, i = 1, 2, 3$ , are the appropriate discretization of the differential operators and the steady state solutions.

Assume that  $B_j, C_j$  are invertible for  $j = 1, 2$ . Solve equations (3.16) and (3.17) for  $U, V$ . Then we find

$$U = (P_4 - P_3P_1^{-1}P_2)H, \quad V = P_1^{-1}P_2H, \quad (3.18)$$

where

$$\begin{aligned} P_1 &= B_2^{-1}B_3 - C_2^{-1}C_3, \\ P_3 &= B_2^{-1}B_3, \\ P_2 &= C_2^{-1}C_1 - B_2^{-1}B_1, \\ P_4 &= -B_2^{-1}B_1. \end{aligned}$$

Then equations (3.15) and (3.18) give an eigenvalue problem as follows:

$$\lambda H + A_1(P_4 - P_3P_1^{-1}P_2)H + A_2P_1^{-1}P_2H = 0. \quad (3.19)$$

Let  $M = A_1(P_4 - P_3P_1^{-1}P_2) + A_2P_1^{-1}P_2$ . Then

$$(\lambda I + M)H = 0, \quad (3.20)$$

where  $I$  is an identity matrix.

Thus, if we could solve the steady state solution to the sheet problem, we could find the eigenvalues of  $M$  and if any of the real parts of those eigenvalues were positive, that solution would be unstable.

## 4 Recommended Future Work

The work presented in this paper can be extended in several ways. A careful derivation of the two dimensional sheet problem should lead to a complete system that can be studied with a variation of the methods presented here. In the case of our steady state problem, we could take advantage of an out-of-the-box solver, `bvp4c()`. Though the two-dimensional problem cannot be attacked by a standard solver, one could write a finite element scheme to handle both the movable boundaries and the non-linearities of the system. Once a steady state solver is implemented, the stability analysis should proceed more closely to the techniques used in this report. The time-dependency would only be present in one of the three governing equations, and thus the ad-hoc method of an Euler Step followed by an steady state update would work just as well in the two-dimensional case as in the one-dimensional case. The eigenvalue scheme could also be formulated and used to find crossover thickness ratios. However, the numerical instabilities that were seen in small ways in the one dimensional case will grow when more inverse matrices must be explicitly formed.

## 5 Acknowledgements

The authors would like to thank Balram Suman for valuable information and insight. We would also like to thank Fadil Santosa, Richard Braun, Holly Pinkerton, and the Institute for Mathematics and Its Applications for facilitating this research project.

## References

- German, R., Khayat, R., and Cui, J. K. *Influence of Inertia and Gravity on the Stability of Filament Jet Flow*, Phys. Fluids, 18, 064108, 2006.
- Howell, P. D. *Models for Thin Viscous Sheets*, Euro Jnl of Applied Mathematics, vol. 7, pp. 321-343, 1996.
- Lamberti, G., Titomanlio, G., and Brucato, V. *Measurement and modelling of the film casting process, 1. Width distribution along draw direction*, Chem. Eng. Science, 56, pp. 5749-5761, 2001.
- Matovich, M. A., Pearson, J. R. A. *Spinning a Molten Threadline: Steady-State Isothermal Viscous Flows*, I&EC Fundamentals, vol. 8, No. 3, August 1969.
- Pearson, J. R. A., Matovich, M. A. *Spinning a Molten Threadline: Stability*, I&EC Fundamentals, vol. 8, No. 4, November 1969.
- Shah, Y. T., and Pearson, J. R. A. *On the stability of non-isothermal fiber spinning - general case*, Industrial and Engineering Chemistry Fundamentals, vol. 11, No. 2, 1972.
- Silagy, D., Demay, Y., and Agassant, J-F. *Study of the Stability of the Film Casting Process*, Polymer Engin. and Science, vol. 36, No. 21, 1996.
- Suman, B. and Kumar, S. *Draw Ratio Enhancement in Non-Isothermal Melt Spinning*, to appear in AIChE Journal, 2008.
- Wylie, J. J., Huang, H., Miura, R. M. *Thermal Instability in Drawing Viscous Threads*, J. Fluid Mech., vol. 570, pp. 1-16, 2007.
- Yeow, Y. L. *On the Stability of Extending Films: A Model for the Film Casting Process*, J. Fluid Mech., vol. 66, Part 21, pp. 613-622, 1974.